

Formation and Phase Transformation of $\text{MgCO}_3 \cdot 3\text{H}_2\text{O}$ Whiskers in the Presence of Sodium Dodecyl Sulfate

Wenting Cheng,* Qianqian Li, Yanxia Wang, Li Fang, and Fangqin Cheng*

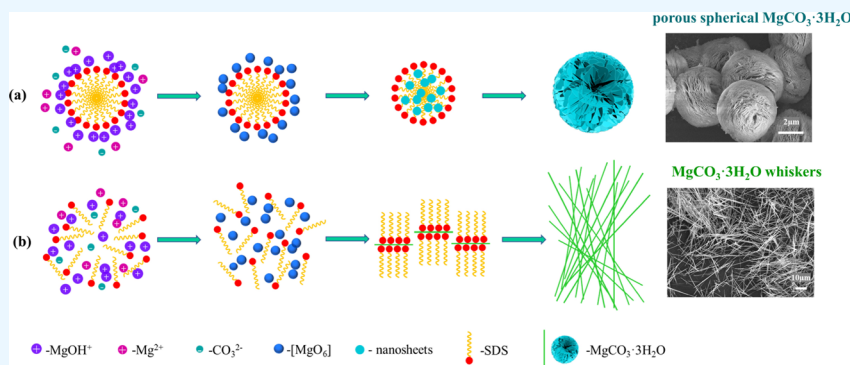
Cite This: *ACS Omega* 2023, 8, 14621–14629

Read Online

ACCESS |

Metrics & More

Article Recommendations



ABSTRACT: Huge amounts of $\text{MgCl}_2 \cdot 6\text{H}_2\text{O}$ are produced annually as a byproduct or waste from KCl production in the Qinghai province of China. An ecological and economic way to solve this problem is transforming the abandoned $\text{MgCl}_2 \cdot 6\text{H}_2\text{O}$ to valuable $\text{MgCO}_3 \cdot 3\text{H}_2\text{O}$ whiskers. The formation and phase transformation of $\text{MgCO}_3 \cdot 3\text{H}_2\text{O}$ whiskers were studied in the crystallization process, in which MgCl_2 and NH_4HCO_3 were precipitated in the presence of sodium dodecyl sulfate (SDS) at 50 °C. Results showed that porous spherical $\text{MgCO}_3 \cdot 3\text{H}_2\text{O}$, $\text{MgCO}_3 \cdot 3\text{H}_2\text{O}$ whiskers, and flocculent rod-like $4\text{MgCO}_3 \cdot \text{Mg}(\text{OH})_2 \cdot 4\text{H}_2\text{O}$ were formed with decreasing concentration of SDS as the crystallization proceeded. When the concentration of SDS was lower than the critical micellar concentration ($6.5 \text{ mmol} \cdot \text{L}^{-1}$) at 60 min, SDS was beneficial for the growth in the [010] direction to form one-dimensional $\text{MgCO}_3 \cdot 3\text{H}_2\text{O}$ whiskers with a high aspect ratio, good uniformity, and a smooth surface (length, 60–70 μm ; aspect ratio, 110–140).

1. INTRODUCTION

30 million tons of $\text{MgCl}_2 \cdot 6\text{H}_2\text{O}$ are produced annually as a byproduct or waste from KCl production in the Qinghai province of China.^{1,2} The huge amount of $\text{MgCl}_2 \cdot 6\text{H}_2\text{O}$ is usually discarded back into the saline lakes,^{1,2} which not only limits the effective and comprehensive utilization of magnesite resource but also causes land occupation and environmental issues. Therefore, it is an ecological and economic way to solve the problem by transforming the abandoned $\text{MgCl}_2 \cdot 6\text{H}_2\text{O}$ to some valuable Mg products.

As one of the high value-added functional materials, $\text{MgCO}_3 \cdot 3\text{H}_2\text{O}$ whiskers could be effectively used as reinforcement fillers in the fields of plastics, coatings, rubber, glass, ceramics, and printing industries due to their excellent physical, chemical, and mechanical properties.^{3,4} Thus, it is much expected to obtain $\text{MgCO}_3 \cdot 3\text{H}_2\text{O}$ whiskers with a high aspect ratio and good uniformity.^{2,5}

$\text{MgCO}_3 \cdot 3\text{H}_2\text{O}$ whiskers are often prepared by crystallization through the reaction of $\text{MgCl}_2 \cdot 6\text{H}_2\text{O}$ with carbonate salts in aqueous solution.^{2,6–9} During crystallization, the crystal size and behavior of the product can be tailored by introducing

surfactants which has an impact on the progress of crystallization.^{2,10} Ionic surfactants are more frequently used than nonionic surfactants because of the strong ionic interaction between crystal sites and surfactant head groups.^{11–13} For example, Singh et al.¹¹ found that the prepared $\text{CuSO}_4 \cdot 5\text{H}_2\text{O}$ crystals were flake-like in visual appearance and formation of layers in the presence of sodium dodecyl sulfate (SDS), whereas it formed prismatic structures and had smooth faces without any surfactant. Shen et al.¹² reported that the increasing SDS concentration caused the morphologies of CaCO_3 aggregates to change from the flower-shaped calcite to hollow spherical calcite and then to solid spherical vaterite. Wei et al.¹³ also reported that CaCO_3

Received: January 22, 2023

Accepted: April 6, 2023

Published: April 14, 2023



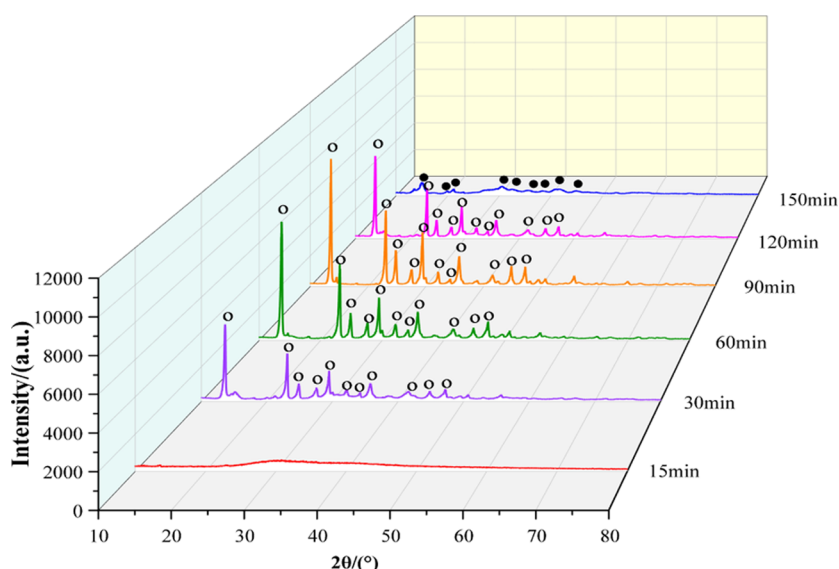


Figure 1. XRD patterns of solid phase generated at different times of crystallization process without SDS: ●- $4\text{MgCO}_3\cdot\text{Mg}(\text{OH})_2\cdot 4\text{H}_2\text{O}$; ○- $\text{MgCO}_3\cdot 3\text{H}_2\text{O}$.

formed very small ($0.5\ \mu\text{m}$) prismatic crystals in the presence of SDS, whereas it formed flat sheets or even flower-like structures if polyvinylpyrrolidone was present along with SDS. But only a very few reports² had discussed the effect of SDS on crystallization of $\text{MgCO}_3\cdot 3\text{H}_2\text{O}$ whiskers. For example, Yang et al.² showed that the presence of SDS in the mixed aqueous solution was an important parameter for the morphology and size of $\text{MgCO}_3\cdot 3\text{H}_2\text{O}$ whiskers. The morphology of $\text{MgCO}_3\cdot 3\text{H}_2\text{O}$ whiskers changed from rod-like to bundle-like with increasing SDS concentration. The above study mainly focused on the effect of SDS concentration, reaction time, and temperature on the morphology of $\text{MgCO}_3\cdot 3\text{H}_2\text{O}$ whiskers. However, the systematic understandings of the formation and phase transformation of $\text{MgCO}_3\cdot 3\text{H}_2\text{O}$ whiskers in the process of crystallization with SDS were still unclear.

In this work, $\text{MgCO}_3\cdot 3\text{H}_2\text{O}$ whiskers were prepared by the reaction of MgCl_2 and NH_4HCO_3 in the presence of SDS at $50\ ^\circ\text{C}$. The effect of SDS on the formation and phase transformation of $\text{MgCO}_3\cdot 3\text{H}_2\text{O}$ whiskers was investigated by monitoring the pH value and the concentration of SDS in solution, determining the critical micellar concentration (CMC) of SDS, analyzing the composition and morphology of the solid phase in the process of crystallization. Besides, $\text{MgCO}_3\cdot 3\text{H}_2\text{O}$ whiskers with a high aspect ratio, good uniformity, and a smooth surface were prepared successfully. Moreover, the formation and transformation mechanisms of $\text{MgCO}_3\cdot 3\text{H}_2\text{O}$ whiskers were studied on the basis of above investigations.

2. EXPERIMENTAL SECTION

2.1. Experimental Materials. Chemical reagents, $\text{MgCl}_2\cdot 6\text{H}_2\text{O}$, NH_4HCO_3 , aqueous $\text{NH}_3\cdot \text{H}_2\text{O}$, SDS, toluene, and acridine orange were analytical grade and purchased from Sinopharm Chemical Reagent Co., Ltd., China. All chemicals were used directly in the experiments without further treatment. The water used in all experimental work for solution preparation, dilution, washing, and so forth was 99.9% double distilled water (conductivity $< 0.1\ \mu\text{S}\cdot\text{cm}^{-1}$).

2.2. Crystallization. The experiments were performed in a batch stirred crystallizer (1 L). MgCl_2 solution (100 mL, 0.5

$\text{mol}\cdot\text{L}^{-1}$) and desired quantity of SDS powder (0 or $0.75\ \text{g}$) were poured into the reactor and stirring at 350 rpm, and then, the solution was brought to $50\ ^\circ\text{C}$ with the aid of the circulating water. Subsequently, the pH adjusted NH_4HCO_3 solution (100 mL, $1\ \text{mol}\cdot\text{L}^{-1}$, pH = 10) via $\text{NH}_3\cdot \text{H}_2\text{O}$ solution was titrated into the reactor by a peristaltic pump and completed after 60 min. After the titration procedure, stirring continued for 90 min. Solid and liquid samples were taken at different times during the experiments. All the samples were filtered immediately with membrane filters ($0.45\ \mu\text{m}$) after sampling, and crystals were washed with deionized water three times and dried at $35\ ^\circ\text{C}$ for more than 12 h.

All the crystallization experiments discussed in this work were carried out with an identical concentration of MgCl_2 and NH_4HCO_3 solutions at $50\ ^\circ\text{C}$. Several trial runs had been conducted with and without SDS to analyze the different growth processes of $\text{MgCO}_3\cdot 3\text{H}_2\text{O}$ crystals.

2.3. Measurement of CMC of SDS with Different pH Values. The CMC of SDS at different pH values was measured by conductivity method^{14–16} for its good stability and sensitivity. The experimental procedure was described briefly below. The $\text{NH}_3\cdot \text{H}_2\text{O}$ solution with desired pH value was prepared at $50\ ^\circ\text{C}$. Then, a certain amount of SDS was added to the solution and continuously stirred for 1 h to ensure well-mixed. After that, the electrical conductivity of the solution was recorded using a conductivity meter. The electrical conductivities of every solution were measured three times to assess the accuracy and reproducibility of the apparatus and procedure described above. The recorded conductivity data were plotted against the corresponding concentration of SDS, and the obvious breaking point at a certain concentration was considered the CMC of SDS with a certain pH value.

2.4. Measurement of Concentration of SDS in Solution. The concentration of SDS in solution was measured using the acridine orange method.^{17,18} This method was based on the extraction of a yellow-colored complex (dodecyl sulfate–acridine orange complex) from aqueous solution into toluene, which could be quantified using UV–visible spectroscopy. The method was described as follows: $100\ \mu\text{L}$ of 1%

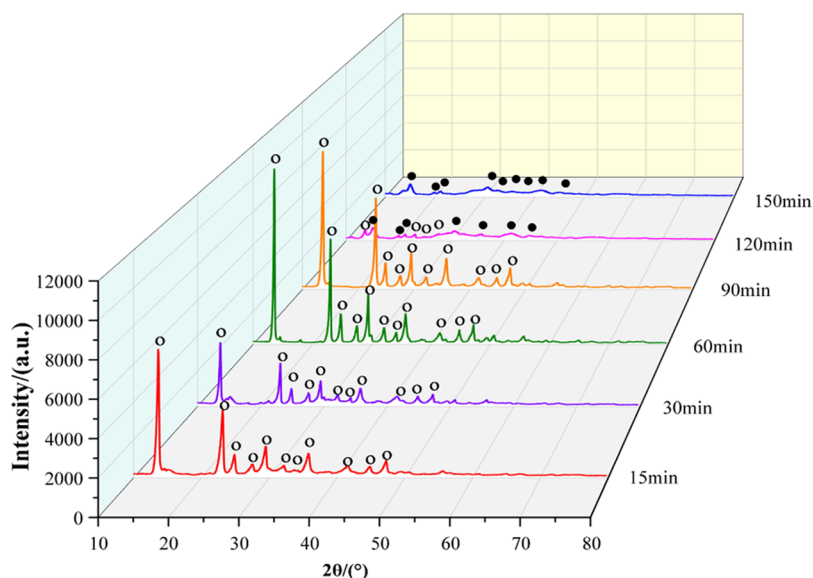


Figure 2. XRD patterns of the solid phase generated at different times of the crystallization process with SDS: ●- $4\text{MgCO}_3\cdot\text{Mg}(\text{OH})_2\cdot 4\text{H}_2\text{O}$; ○- $\text{MgCO}_3\cdot 3\text{H}_2\text{O}$.

Table 1. Composition of the Solid Phase Generated at Different Times of the Crystallization Process with and without SDS

reaction time (min)	solid phase (without SDS)	solid phase (with SDS)
15	amorphism	$\text{MgCO}_3\cdot 3\text{H}_2\text{O}$
30	$\text{MgCO}_3\cdot 3\text{H}_2\text{O}$	$\text{MgCO}_3\cdot 3\text{H}_2\text{O}$
60	$\text{MgCO}_3\cdot 3\text{H}_2\text{O}$	$\text{MgCO}_3\cdot 3\text{H}_2\text{O}$
90	$\text{MgCO}_3\cdot 3\text{H}_2\text{O}$	$\text{MgCO}_3\cdot 3\text{H}_2\text{O}$
120	$\text{MgCO}_3\cdot 3\text{H}_2\text{O}$	$\text{MgCO}_3\cdot 3\text{H}_2\text{O}$, $4\text{MgCO}_3\cdot\text{Mg}(\text{OH})_2\cdot 4\text{H}_2\text{O}$
150	$4\text{MgCO}_3\cdot\text{Mg}(\text{OH})_2\cdot 4\text{H}_2\text{O}$	$4\text{MgCO}_3\cdot\text{Mg}(\text{OH})_2\cdot 4\text{H}_2\text{O}$

acridine orange was added to 100 μL of SDS solution and shaken for 2 min. The yellow-colored complex was then extracted using 5 mL of toluene by shaking for 3 min and settling for 5 min. The toluene layer was collected and then analyzed using UV–vis spectroscopy against a calibration curve to determine the concentration of SDS.

2.5. Characterization. During each experimental run, the pH values of the solution were monitored by a pH meter (Denver instrument UB-7, Germany). The electrical conductivities of the solution were recorded using a conductivity meter (Mettler Toledo, FE38-Standard, China). Spectroscopic measurements were obtained using a spectrophotometer (Shimadzu, UV-2600, China). The compositions of samples were analyzed by X-ray powder diffractometer (XRD, Bruker D2PHASERX, Germany) using $\text{Cu K}\alpha$ radiation, operating at 40 kV, 30 mA, and a scanning rate of $0.02^\circ\cdot\text{s}^{-1}$ from 10 to 80° . The morphologies of samples were observed by scanning electron microscopy (JSM-IT500HR, Japan), and the size of particles obtained from counting 100 crystals observed in SEM images.

3. RESULTS AND DISCUSSION

3.1. Effect of SDS on the Phase Transformation of $\text{MgCO}_3\cdot 3\text{H}_2\text{O}$. The XRD patterns of the solid phase generated at different reaction times of crystallization process without and with SDS are shown in Figures 1 and 2. As could be seen from Figure 1, at the beginning of crystallization process without SDS (15 min), the corresponding XRD pattern had no obvious diffraction peaks, indicating that it was the amorphous phase. When the reaction time was 30 min, there were some

weak diffraction peaks of $\text{MgCO}_3\cdot 3\text{H}_2\text{O}$ (JCPDS 20-0669), indicating the poor crystallization. From 60 to 90 min, some diffraction peaks (JCPDS 20-0669) could be seen and then become stronger in the XRD patterns indicating that the $\text{MgCO}_3\cdot 3\text{H}_2\text{O}$ crystals gradually crystallized. As the reaction time extended to 120 min, the diffraction peaks of $\text{MgCO}_3\cdot 3\text{H}_2\text{O}$ crystals became weaker illustrating that the crystallinity was decreased. When the reaction time was further prolonged to 150 min, the diffraction peaks of $\text{MgCO}_3\cdot 3\text{H}_2\text{O}$ disappeared and were displaced by the diffraction peaks of $4\text{MgCO}_3\cdot\text{Mg}(\text{OH})_2\cdot 4\text{H}_2\text{O}$ (JCPDS 25-0513), which indicating the transformation happened.

In contrast, at the beginning of crystallization process with SDS (15 min), all of the diffraction peaks in the XRD patterns were matched with the standard JCPDS 20-0669 of $\text{MgCO}_3\cdot 3\text{H}_2\text{O}$ (Figure 2). It was verified that the presence of SDS promoted the formation of $\text{MgCO}_3\cdot 3\text{H}_2\text{O}$ compared with the amorphous phase in Figure 1. At the reaction time of 30 min, the diffraction peaks of $\text{MgCO}_3\cdot 3\text{H}_2\text{O}$ (JCPDS 20-0669) crystals decreased, indicating lower crystallinity. This case might be due to the change of the crystal morphology caused by the decrease of SDS concentration during the titration process. From 60 to 90 min, the solid phases obtained with SDS were also $\text{MgCO}_3\cdot 3\text{H}_2\text{O}$ crystals, but some of the diffraction peaks, for example, (101) at 13.6° and (002) at 23.1° were obviously much stronger than these crystals obtained without SDS. This case indicated that SDS might promote the growth of special faces of crystals. The diffraction peaks of $\text{MgCO}_3\cdot 3\text{H}_2\text{O}$ crystals also became weaker with the time elapsed but some of the diffraction peaks of $4\text{MgCO}_3\cdot$

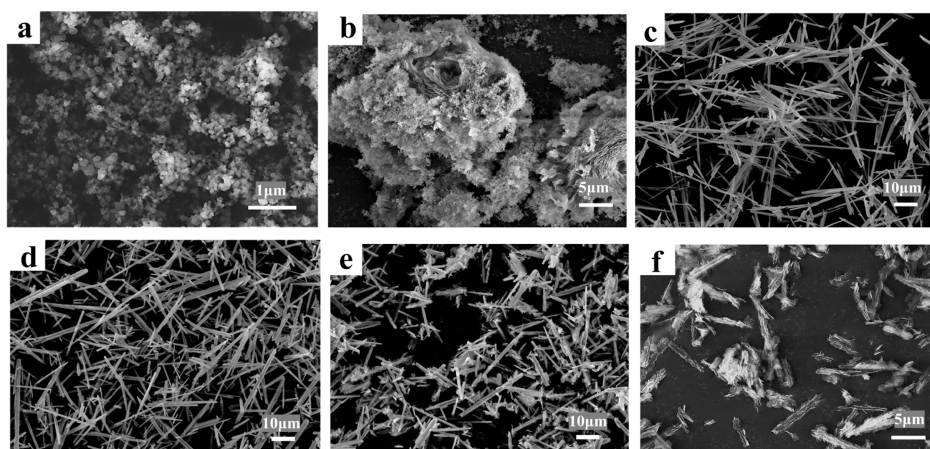


Figure 3. SEM images of the solid phase generated at different times of the crystallization process without SDS: (a) 15; (b) 30; (c) 60; (d) 90; (e) 120; and (f) 150 min.

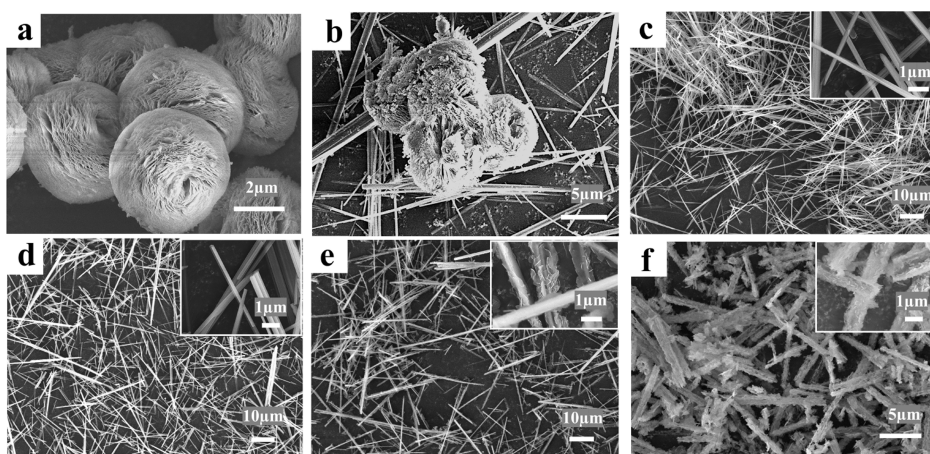


Figure 4. SEM images of the solid phase generated at different times of the crystallization process in the presence of SDS: (a) 15; (b) 30; (c) 60; (d) 90; (e) 120; and (f) 150 min.

$\text{Mg}(\text{OH})_2 \cdot 4\text{H}_2\text{O}$ (JCPDS 25-0513) generated earlier at 120 min and then the diffraction peaks of $\text{MgCO}_3 \cdot 3\text{H}_2\text{O}$ disappeared completely after 150 min. Solid phases generated at different times of crystallization process without and with SDS are listed in Table 1 for a clear comparison. It was verified that SDS apparently enhanced the formation and transformation of $\text{MgCO}_3 \cdot 3\text{H}_2\text{O}$ crystals in the whole crystallization process.

3.2. Effect of SDS on the Morphology of $\text{MgCO}_3 \cdot 3\text{H}_2\text{O}$ Crystals. Although the effect of some surfactants on crystal morphology was well discussed in the literature,^{10–13} the specific system was not explored systematically. Hence, the effect of SDS on the morphology of $\text{MgCO}_3 \cdot 3\text{H}_2\text{O}$ whiskers was briefly discussed in the formation and transformation process. The morphology evolutions of the solid phase without and with SDS were examined by SEM observations (Figures 3 and 4).

As can be seen from Figure 3, at the beginning of crystallization process without SDS (15 min), the morphology of the corresponding solid phase was amorphous. When the reaction time was 30 min, it could be seen that several porous and flower-like $\text{MgCO}_3 \cdot 3\text{H}_2\text{O}$ generated from the amorphous grains. From 60 to 90 min, the whisker-like $\text{MgCO}_3 \cdot 3\text{H}_2\text{O}$ crystals obtained and grew larger with the increased time. However, these whisker-like $\text{MgCO}_3 \cdot 3\text{H}_2\text{O}$ crystals had

irregular size and low aspect ratio. For example, the length and the aspect ratio of the crystals obtained at 60 min were 21–27 μm and 20–25, respectively. Meanwhile, the length and the aspect ratio of the crystals obtained at 90 min only increased to 26–36 μm and 32–38, respectively. As the reaction time extended to 120 min, some lamellar and floc crystals generated gradually on the surface of the rod-like $\text{MgCO}_3 \cdot 3\text{H}_2\text{O}$ crystals. Then, all the rod-like crystals were displaced by lamellar and floc crystals with the reaction time further prolonged to 150 min, indicating complete phase transformation from $\text{MgCO}_3 \cdot 3\text{H}_2\text{O}$ to $4\text{MgCO}_3 \cdot \text{Mg}(\text{OH})_2 \cdot 4\text{H}_2\text{O}$.

In contrast, at the beginning of the crystallization process in the presence of SDS (15 min), the morphology of the corresponding solid phase was porous spherical $\text{MgCO}_3 \cdot 3\text{H}_2\text{O}$ which consisted of nanosheets. The average diameter of the spherical crystals was 5 μm . It was illustrated that SDS could promote the formation of porous spherical $\text{MgCO}_3 \cdot 3\text{H}_2\text{O}$ by adjusting the arrangement of nanocrystals. This case might be because the first surfactant structures that formed in a surfactant solution were spherical micelles.^{19,20} Then, the spherical crystals decreased and became cracked while some rod-like crystals appeared at 30 min. This case led to the decrease in crystallinity as can be seen in the XRD pattern of $\text{MgCO}_3 \cdot 3\text{H}_2\text{O}$ crystals (Figure 2). From 60 to 90 min, all the

$\text{MgCO}_3 \cdot 3\text{H}_2\text{O}$ crystals were whisker-like with a high aspect ratio and smooth surface. It was illustrated that the SDS promoted regulation growth of $\text{MgCO}_3 \cdot 3\text{H}_2\text{O}$ crystals along the one-dimensional direction.² The most prominent effect of SDS was observed at 60 min when $\text{MgCO}_3 \cdot 3\text{H}_2\text{O}$ whiskers formed with the length of 60–70 μm and aspect ratio of 110–140. However, further increasing the reaction time up to 90 min resulted in a reduction of the length and the aspect ratio of the crystals, and they decreased to 40–50 μm and 100–110, respectively. With the reaction time extended to 120 min, the smooth surface of $\text{MgCO}_3 \cdot 3\text{H}_2\text{O}$ whiskers became rough and was covered with some lamellar crystals. When the reaction time further extended to 150 min, the obtained products were flocculent rod-like $4\text{MgCO}_3 \cdot \text{Mg}(\text{OH})_2 \cdot 4\text{H}_2\text{O}$ with an average length of 10 μm , indicating complete phase transformation. This case might due to a spontaneous process which named Ostwald ripening²¹ occurred from the outside to inside of $\text{MgCO}_3 \cdot 3\text{H}_2\text{O}$ whiskers with the extension of the reaction time. The large particles on the outer surface of whiskers grew through the consumption of small particles. Flocculent rod-like crystals finally formed when the small particles were completely eroded.

Compared Figure 3 with Figure 4, it could be seen that the SDS had a promotional and structure-direction effect on the formation and transformation of $\text{MgCO}_3 \cdot 3\text{H}_2\text{O}$ crystals. Especially, SDS was obviously beneficial to the formation of $\text{MgCO}_3 \cdot 3\text{H}_2\text{O}$ whiskers with a high aspect ratio, good dispersity, and smooth surface. The prominent effect of SDS on the $\text{MgCO}_3 \cdot 3\text{H}_2\text{O}$ crystals was consistent with the XRD result.

For further exploring the effect of SDS on the formation and transformation of $\text{MgCO}_3 \cdot 3\text{H}_2\text{O}$ crystals, the CMC of SDS in the crystallization process was determined in the following section.

3.3. Determination of CMC of SDS in the Crystallization Process. It is well known that the concentration of the surfactant used in the crystallization process is a critical parameter.^{2,11} The effect of surfactant usually changes with increasing or decreasing its concentration. As crystals form various self-assembled structures in the presence of surfactants in solution, it is important to figure out whether the concentration effect of surfactants is related to the appearance of such structures.

The CMC^{22–25} of the surfactant is the concentration at which monomeric surfactant molecules can thermodynamically self-aggregate, forming the molecular aggregates called micelles. In other words, the CMC of surfactant is the concentration at which the micelle makes its appearance. It was reported that the CMC of surfactant was different with various pH values.^{26–28} Jiang et al.²⁶ proposed that the pH was a complex factor which affected surface properties of dodecyltrimethylammonium decanoate. Mitra et al.²⁷ found that the CMC of quillaja saponin increased monotonically with aqueous phase pH in the pH range of 3.0–8.8, and the increase in CMC was most significant at pH = 8.8. Song et al.²⁸ explored the effect of pH on the CMC of TX-100/DDAO mixed surfactant system. Results showed that the CMC of binary TX-100/DDAO solution decreased with the decrease in pH in the range pH > 5.03 while increased with the decrease in pH in the range pH < 5.03.

Therefore, the pH value of $\text{MgCO}_3 \cdot 3\text{H}_2\text{O}$ crystallization system was tracked and monitored along with the reaction time primarily. As Figure 5 showed, the pH value increased

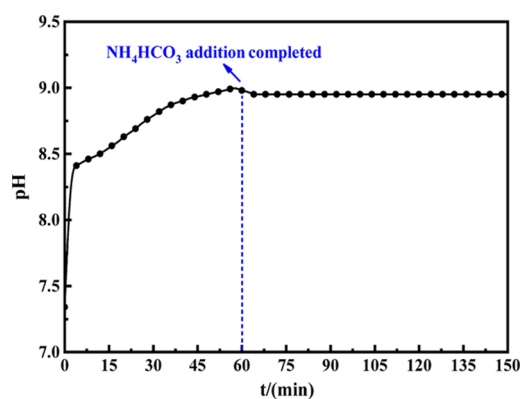


Figure 5. pH value in the $\text{MgCO}_3 \cdot 3\text{H}_2\text{O}$ crystallization system at different times.

sharply from 7.3 to 8.5 and then increased smoothly from 8.5 to 9.0 with NH_4HCO_3 addition time of 0–60 min. After titration, the pH value had a slightly decrease and then keep at 8.9 after 63 min. In a word, the pH value was in the range of 7.3–9.0 in the whole crystallization process. Therefore, the CMC of SDS in $\text{NH}_3 \cdot \text{H}_2\text{O}$ solution was determined, respectively, at pH = 7, 8, and 9 by the conductivity method.

Before above work, the experimentally obtained values of CMC for SDS in water at different temperatures were compared with some of the literature^{22–25} to assess the accuracy of the using determination method. The gradual decrease in the slope and a break in the plot gave the value of CMC as given in Figure 6. The result (Table 2) showed that the experimental data agreed well with the published CMC values.

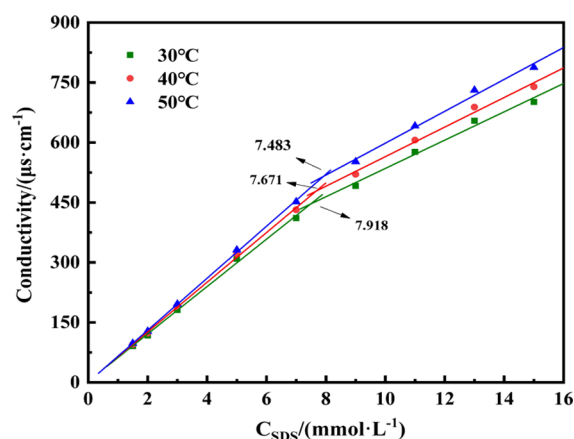


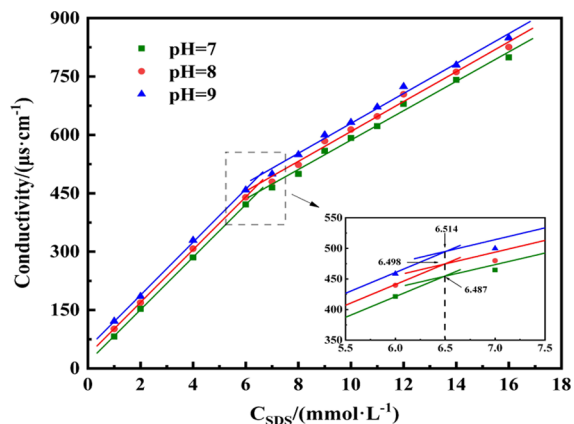
Figure 6. CMC of SDS in water at different temperatures.

From Figure 7 it was noticed that the slight increase of CMC took place with the increase of the pH value. For example, the CMC merely increased from 6.487 to 6.498 to 6.514 $\text{mmol} \cdot \text{L}^{-1}$ as the pH value increased from 7 to 8 to 9. This case might be due to the narrow change of pH values was not enough to influence the CMC. In other words, the CMC of SDS has no significant dependence on pH values in a narrow range of 7–9. It is decided to use the average CMC value of 6.5 $\text{mmol} \cdot \text{L}^{-1}$ in the whole crystallization process.

3.4. Formation and Transformation Mechanisms of $\text{MgCO}_3 \cdot 3\text{H}_2\text{O}$ Whiskers. The structure of $\text{MgCO}_3 \cdot 3\text{H}_2\text{O}$ crystal is formed by twisted $[\text{MgO}_6]$ regular octahedrons

Table 2. Comparison of Experimentally Obtained and Literature Values of CMC for SDS in Water at Different Temperatures

temperatures (°C)	CMC (mmol·L ⁻¹) for SDS				
	experimental	literature ²²	literature ²³	literature ²⁴	literature ²⁵
30	7.483	7.68	7.97	7.04	8.3
40	7.671		7.08	7.37	8.7
50	7.918			7.80	

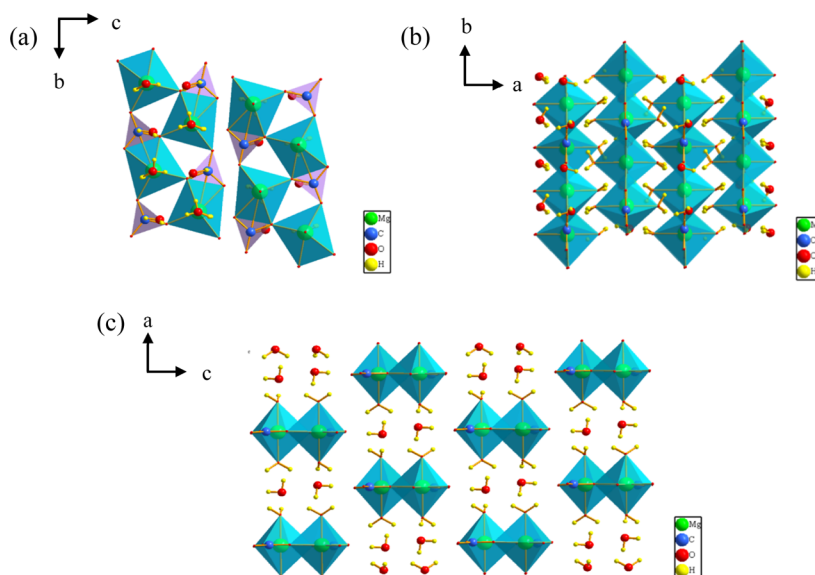
Figure 7. CMC of SDS in NH₃·H₂O solution at different pH values.

connected in a common vertex connection.^{29,30} For example, the [MgO₆] regular octahedrons are connected by Mg–O and C–O bonds along the [100] and [001] directions with a common vertex or common prism (Figure 8a,b). In the [010] direction, the [MgO₆] regular octahedrons are connected by the Mg–O bonds in a common vertex manner (Figure 8c). According to the Pauling rule,^{21,31} the growth surfaces of [MgO₆] regular octahedrons connect by the vertex-sharing or edge-sharing, especially the planes-sharing, will reduce the stability of the coordination crystal structure and sequentially decrease the growth rate. Therefore, the growth unit of [MgO₆] regular octahedron will spontaneously grow fastest along the [010] direction. MgCO₃·3H₂O crystals will form

with a relatively stable one-dimensional rod-like structure if there is no external driving force.

However, it was concluded from the foregoing discussions that the crystallization process in the presence of SDS could be divided into three stages: (I) formation of porous spherical MgCO₃·3H₂O, (II) transformation from porous spherical MgCO₃·3H₂O to MgCO₃·3H₂O whiskers, and (III) transformation from MgCO₃·3H₂O whiskers to flocculent rod-like 4MgCO₃·Mg(OH)₂·4H₂O. The concentration of SDS had a significant effect on the formation and transformation of MgCO₃·3H₂O crystals. The above stages are shown in Figure 9 where the solid line indicated the concentration of SDS and the dotted line indicated the CMC of SDS during the crystallization process.

It can be seen from Figure 9 that at the beginning of stage (I), the initial concentration of SDS in the solution before titration was 10.2 mmol·L⁻¹, which was much higher than CMC (6.5 mmol·L⁻¹). Thus, the SDS existed in the form of micelles before crystallization. When the NH₄HCO₃ solution (pH = 10) titration started, MgOH⁺ ions were formed by Mg²⁺ and OH⁻ ions, and the MgOH⁺ ions were attached with the SDS micelles surfaces for their strong negative polarity. Then, the regular octahedral growth units of [MgO₆] were formed by MgOH⁺ and CO₃²⁻ ions. The growth units entered from the surfaces into the micelles and formed nanosheets via synergism and cooperation.³² Besides, the nanosheets took the micelles as the templates to form spherical structure through aggregation and superposition. Moreover, the nanosheets could only grow along two-dimensional directions to form porous spherical MgCO₃·3H₂O due to the inhibition of SDS micelle on the

Figure 8. Crystal structure of MgCO₃·3H₂O: (a) in projection parallel to [100], (b) in projection parallel to [001], and (c) in projection parallel to [010].

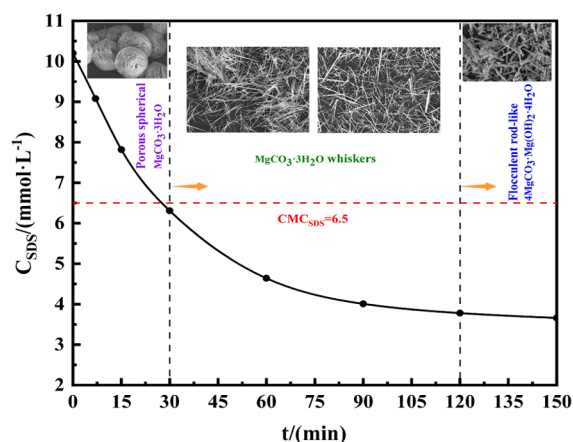


Figure 9. Concentration and CMC of SDS during the crystallization process.

crystal plane. The scheme of formation mechanism of porous spherical $\text{MgCO}_3 \cdot 3\text{H}_2\text{O}$ is illustrated in Figure 10a.

With the titration of NH_4HCO_3 solution, the concentration of SDS decreased gradually toward the CMC ($6.5 \text{ mmol} \cdot \text{L}^{-1}$). At the beginning of stage (II), the concentration of SDS ($6.31 \text{ mmol} \cdot \text{L}^{-1}$) was lower than CMC at 30 min. The SDS micelles gradually disintegrated and the inhibition of them on the crystal plane weakened accordingly. Meanwhile, some of the regular octahedron growth units of $[\text{MgO}_6]$ grew along the $[010]$ direction spontaneously. Therefore, the porous spherical $\text{MgCO}_3 \cdot 3\text{H}_2\text{O}$ cracked and broke, while some rod-like $\text{MgCO}_3 \cdot 3\text{H}_2\text{O}$ appeared. At the one-third time of stage (II) (60 min), with the further decrease of the concentration of SDS, the SDS micelles disintegrated completely and directional arranged on the $\text{MgCO}_3 \cdot 3\text{H}_2\text{O}$ crystal nuclei surface after adsorption. This case created a separation of active ions from the surface, which could inhibit the growth, agglomeration, and secondary nucleation in the $[100]$ and $[001]$ directions. As a result, it could promote the growth in the $[010]$ direction to form one-dimensional $\text{MgCO}_3 \cdot 3\text{H}_2\text{O}$ whiskers with a high aspect ratio and smooth surface. At the two-third time of stage (II) (90 min), the inhibition effect of SDS weakened due to its continuously consumption, which resulted in a reduce of the average length and the aspect ratio of the $\text{MgCO}_3 \cdot 3\text{H}_2\text{O}$

whiskers. The scheme of formation mechanism of $\text{MgCO}_3 \cdot 3\text{H}_2\text{O}$ whiskers is illustrated in Figure 10b.

At the stage (III), the $\text{MgCO}_3 \cdot 3\text{H}_2\text{O}$ whiskers gradually transformed to flocculent rod-like $4\text{MgCO}_3 \cdot \text{Mg}(\text{OH})_2 \cdot 4\text{H}_2\text{O}$. This case could be explained by the structural stability of the two hydrated magnesium carbonates. In the crystal structure of $4\text{MgCO}_3 \cdot \text{Mg}(\text{OH})_2 \cdot 4\text{H}_2\text{O}$,³⁰ there are two different $[\text{MgO}_6]$ octahedrons formed by the octahedral-coordination of Mg^{2+} (Figure 11). The two coordination octahedrons are joined by

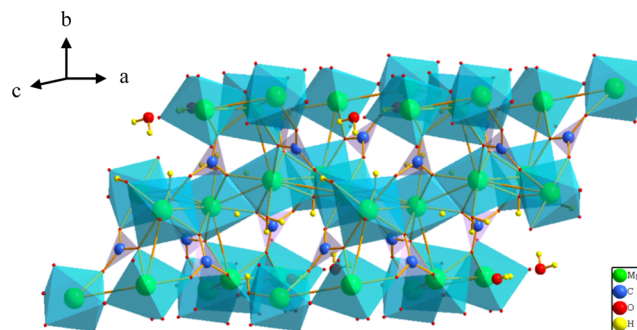


Figure 11. Crystal structure of $4\text{MgCO}_3 \cdot \text{Mg}(\text{OH})_2 \cdot 4\text{H}_2\text{O}$.

$[\text{CO}_3]$ triangles or co-vertices or co-edges, and the total number of vertices is less than that in the structure of $\text{MgCO}_3 \cdot 3\text{H}_2\text{O}$ (Figure 8). Pauling rule^{21,31} points out that in the coordination structure, the distance of the central cations is lengthened by the reduce of the number of common vertices. Moreover, the Coulomb repulsion of the central cations will be weakened, which can lead to a strengthen of the structural stability. Therefore, the structural stability of $4\text{MgCO}_3 \cdot \text{Mg}(\text{OH})_2 \cdot 4\text{H}_2\text{O}$ is higher than $\text{MgCO}_3 \cdot 3\text{H}_2\text{O}$. $\text{MgCO}_3 \cdot 3\text{H}_2\text{O}$ was in a metastable state of hydrated magnesium carbonate at 50°C . The unstable $\text{MgCO}_3 \cdot 3\text{H}_2\text{O}$ would eventually transform to the stable $4\text{MgCO}_3 \cdot \text{Mg}(\text{OH})_2 \cdot 4\text{H}_2\text{O}$ when the reaction time was extended at 150 min.

4. CONCLUSIONS

The phase composition and morphology of solids obtained during the crystallization process using MgCl_2 and NH_4HCO_3 as raw materials were investigated without and with SDS at 50°C . The presence of SDS showed obvious promotion in the

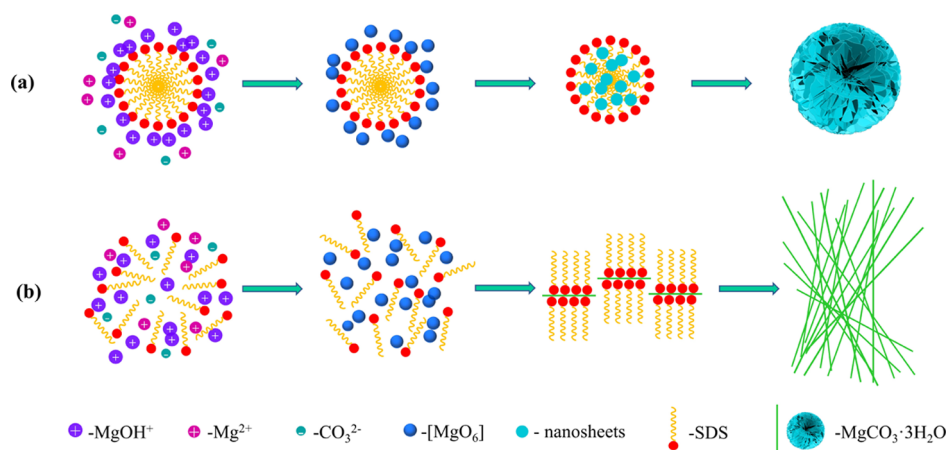


Figure 10. Schematic representation of morphology evolution in the $\text{MgCO}_3 \cdot 3\text{H}_2\text{O}$ formation process: (a) formation of porous spherical $\text{MgCO}_3 \cdot 3\text{H}_2\text{O}$ and (b) formation of $\text{MgCO}_3 \cdot 3\text{H}_2\text{O}$ whiskers.

regulated formation and transformation of $\text{MgCO}_3 \cdot 3\text{H}_2\text{O}$ crystals.

The measured average CMC value of SDS in the whole crystallization process was $6.5 \text{ mmol} \cdot \text{L}^{-1}$. When the concentration of SDS was much higher than CMC at 15 min, porous spherical $\text{MgCO}_3 \cdot 3\text{H}_2\text{O}$ was obtained using SDS micelle as a template. When the concentration of SDS was lower than CMC after 30 min, SDS micelle gradually disintegrated and promoted the growth in the [010] direction to form one-dimensional $\text{MgCO}_3 \cdot 3\text{H}_2\text{O}$ whiskers. $\text{MgCO}_3 \cdot 3\text{H}_2\text{O}$ whiskers with a high aspect ratio, good uniformity, and smooth surface (length of 60–70 μm and aspect ratio of 110–140) were prepared at 60 min. When the reaction time was extended to 120 min, the $\text{MgCO}_3 \cdot 3\text{H}_2\text{O}$ whiskers would gradually transform to flocculent rod-like $4\text{MgCO}_3 \cdot \text{Mg}(\text{OH})_2 \cdot 4\text{H}_2\text{O}$. This case was because $4\text{MgCO}_3 \cdot \text{Mg}(\text{OH})_2 \cdot 4\text{H}_2\text{O}$ had stronger stability due to its less number of vertices in the structure compared with $\text{MgCO}_3 \cdot 3\text{H}_2\text{O}$. These findings could pave the way for controllable crystallization of $\text{MgCO}_3 \cdot 3\text{H}_2\text{O}$ whiskers with a high aspect ratio, good uniformity, and a smooth surface.

AUTHOR INFORMATION

Corresponding Authors

Wenting Cheng – Institute of Resources and Environmental Engineering, State Environmental Protection Key Laboratory of Efficient Utilization Technology of Coal Waste Resources, Shanxi University, Taiyuan, Shanxi 030006, China;
orcid.org/0000-0001-8624-6471; Email: wtcheng@sxu.edu.cn

Fangqin Cheng – Institute of Resources and Environmental Engineering, State Environmental Protection Key Laboratory of Efficient Utilization Technology of Coal Waste Resources, Shanxi University, Taiyuan, Shanxi 030006, China;
orcid.org/0000-0002-2961-2989; Email: cfangqin@sxu.edu.cn

Authors

Qianqian Li – Institute of Resources and Environmental Engineering, State Environmental Protection Key Laboratory of Efficient Utilization Technology of Coal Waste Resources, Shanxi University, Taiyuan, Shanxi 030006, China

Yanxia Wang – Institute of Resources and Environmental Engineering, State Environmental Protection Key Laboratory of Efficient Utilization Technology of Coal Waste Resources, Shanxi University, Taiyuan, Shanxi 030006, China

Li Fang – Institute of Resources and Environmental Engineering, State Environmental Protection Key Laboratory of Efficient Utilization Technology of Coal Waste Resources, Shanxi University, Taiyuan, Shanxi 030006, China

Complete contact information is available at:
<https://pubs.acs.org/10.1021/acsomega.3c00459>

Notes

The authors declare no competing financial interest.

ACKNOWLEDGMENTS

The support of National Natural Science Foundation of China (grant nos. 22208198 and 21A20321) and National Key Research and Development Program (grant no. 2022YFC3901305) are gratefully acknowledged.

REFERENCES

- (1) Wang, J. F.; Li, Z. B. Crystallization and agglomeration kinetics of hydromagnesite in the reactive system $\text{MgCl}_2\text{--Na}_2\text{CO}_3\text{--NaOH--H}_2\text{O}$. *Ind. Eng. Chem. Res.* **2012**, *51*, 7874–7883.
- (2) Yang, C.; Song, X. F.; Sun, S. Y.; Sun, Z.; Yu, J. G. Effects of sodium dodecyl sulfate on the oriented growth of nesquehonite whiskers. *Adv. Powder Technol.* **2013**, *24*, 585–592.
- (3) Zhang, Z. P.; Zheng, Y. J.; Zhang, J. X.; Zhang, Q.; Chen, J. P.; Liu, Z. M.; Liang, X. M. Synthesis and shape evolution of monodisperse basic magnesium carbonate microspheres. *Cryst. Growth Des.* **2007**, *7*, 337–342.
- (4) Zhang, Z. P.; Zheng, Y. J.; Zhang, J. X.; Chen, J. P.; Liang, X. M. Magnesium oxide microspheres as a packing material for the separation of basic compounds in normal-phase liquid chromatography. *J. Chromatogr. A* **2007**, *1165*, 116–121.
- (5) Kloprogge, J. T.; Martens, W. N.; Nothdurft, L.; Duong, L. V.; Webb, G. E. Low temperature synthesis and characterization of nesquehonite. *J. Mater. Sci. Lett.* **2003**, *22*, 825–829.
- (6) Wang, X. L.; Xue, D. F. Direct observation of the shape evolution of MgO whiskers in a solution system. *Mater. Lett.* **2006**, *60*, 3160–3164.
- (7) Wang, Y.; Li, Z. B.; Demopoulos, G. P. Controlled precipitation of nesquehonite ($\text{MgCO}_3 \cdot 3\text{H}_2\text{O}$) by the reaction of MgCl_2 with $(\text{NH}_4)_2\text{CO}_3$. *J. Cryst. Growth* **2008**, *310*, 1220–1227.
- (8) Cheng, W. T.; Zhang, C. Y.; Cheng, H. G.; Chen, Z. L.; Liao, H. Q.; Cheng, F. Q. Effect of ethanol on the crystallization and phase transformation of $\text{MgCO}_3 \cdot 3\text{H}_2\text{O}$ in a $\text{MgCl}_2\text{--CO}_2\text{--NH}_3\text{--H}_2\text{O}$ system. *Powder Technol.* **2018**, *335*, 164–170.
- (9) Cheng, W. T.; Bo, Q. F.; Xu, T.; Cheng, F. Synthesis of magnesium oxide assisted by PEG-10000 and adsorption capacity for lead solution. *Sci. China: Chem.* **2013**, *43*, 1490–1496.
- (10) Tierney, T. B.; Rasmuson, A. C.; Hudson, S. P. Size and shape control of micron-sized salicylic acid crystals during antisolvent crystallization. *Org. Process Res. Dev.* **2017**, *21*, 1732–1740.
- (11) Singh, N.; Yeri, R.; Chakraborty, J. Effect of ionic surfactants and alcohols on the morphology of $\text{CuSO}_4 \cdot 5\text{H}_2\text{O}$ crystals: combined use of factors and significance of threshold surfactant concentration. *Ind. Eng. Chem. Res.* **2013**, *52*, 15041–15048.
- (12) Shen, Q.; Wei, H.; Wang, L. C.; Zhou, Y.; Zhao, Y.; Zhang, Z. Q.; Wang, D. J.; Xu, G. Y.; Xu, D. F. Crystallization and aggregation behaviors of calcium carbonate in the presence of poly(vinylpyrrolidone) and sodium dodecyl sulfate. *J. Phys. Chem. B* **2005**, *109*, 18342–18347.
- (13) Wei, H.; Shen, Q.; Zhao, Y.; Wang, D.; Xu, D. Crystallization habit of calcium carbonate in presence of sodium dodecyl sulfate and/or polyvinylpyrrolidone. *J. Cryst. Growth* **2004**, *260*, 545–550.
- (14) Alam, M. M.; Rana, S.; Rub, M. A.; Hoque, M. A.; Kabir, S. E.; Asiri, A. M. Influence of various electrolytes on the interaction of cetyltrimethylammonium bromide with tetradecyltrimethylammonium bromide at different temperatures and compositions: Experimental and theoretical investigation. *J. Mol. Liq.* **2019**, *278*, 86–96.
- (15) Kumar, H.; Katal, A.; Rawat, P. FT-IR spectroscopic and micellization studies of cetyltrimethylammonium bromide in aqueous and aqueous solution of ionic liquid (1-butyl-3-methylimidazolium bromide) at different temperatures. *J. Mol. Liq.* **2018**, *249*, 227–232.
- (16) Kumar, H.; Sharma, N.; Katal, A. Aggregation behaviour of cationic (cetyltrimethylammonium bromide) and anionic (sodium dodecylsulphate) surfactants in aqueous solution of synthesized ionic liquid [1-pentyl-3-methylimidazolium bromide] -Conductivity and FT-IR spectroscopic studies. *J. Mol. Liq.* **2018**, *258*, 285–294.
- (17) Sokoloff, R. L.; Frigon, R. P. Rapid spectrophotometric assay of dodecyl sulfate using acridine orange. *Anal. Biochem.* **1981**, *118*, 138–141.
- (18) Adak, A.; Pal, A.; Bandyopadhyay, M. Spectrophotometric determination of anionic surfactants in wastewater using acridine orange. *Indian J. Chem. Technol.* **2005**, *12*, 145–148.
- (19) Pal, A.; Punia, R. Mixed micellization behaviour of tri-substituted surface active ionic liquid and cationic surfactant in

aqueous medium and salt solution: Experimental and theoretical study. *J. Mol. Liq.* **2019**, *296*, 111831.

(20) Bharmoria, P.; Vaneet; Banipal, P. K.; Kumar, A.; Kang, T. S. Modulation of micellization behavior of cetyltrimethylammonium bromide (CTAB) by organic anions in low concentration regime. *J. Solution Chem.* **2015**, *44*, 16–33.

(21) Wang, Y. L.; Liu, J. Y.; Shi, T. J.; Yang, B.; Li, C.; Xu, H.; Yin, W. Z. Preparation, properties and phase transition of mesoporous hydromagnesite with various morphologies from natural magnesite. *Powder Technol.* **2020**, *364*, 822–830.

(22) Kumar, H.; Katal, A. Thermodynamic analysis of micelles formation of anionic surfactant SDS in the presence of aqueous and aqueous solution of ionic liquid 1-butyl-3-methylimidazolium chloride. *J. Phys. Org. Chem.* **2021**, *34*, 4199.

(23) Mahbub, S.; Mia, M. L.; Roy, T.; Akter, P.; Uddin, A. R.; Rub, M. A.; Hoque, M. A.; Asiri, A. M. Influence of ammonium salts on the interaction of fluoroquinolone antibiotic drug with sodium dodecyl sulfate at different temperatures and compositions. *J. Mol. Liq.* **2020**, *297*, 111583.

(24) Hussain, A.; Shuaibu, A. D.; Shaikh, A. J.; Khan, A. M. Exploring the effects of selected essential amino acids on the self-association of sodium dodecyl sulphate at different temperatures. *J. Mol. Liq.* **2022**, *347*, 118003.

(25) Das, D.; Ismail, K. Aggregation and adsorption properties of sodium dodecyl sulfate in water–acetamide mixtures. *J. Colloid Interface Sci.* **2008**, *327*, 198–203.

(26) Jiang, Y. J.; Geng, T.; Li, Q. X.; Li, G. J.; Ju, H. B. Influences of temperature, pH and salinity on the surface property and self-assembly of 1:1 salt-free catanionic surfactant. *J. Mol. Liq.* **2014**, *199*, 1–6.

(27) Mitra, S.; Dungan, S. R. Micellar properties of quillaja saponin. I. Effects of temperature, salt, and pH on solution properties. *J. Agric. Food Chem.* **1997**, *45*, 1587–1595.

(28) Song, S. L.; Hu, Z. G.; Qian, Y. H.; Chen, Z.; Zhang, G. Properties of surface and micelle in a pH-mediated ternary surfactant mixture in salt solution. *J. Dispersion Sci. Technol.* **2006**, *27*, 907–913.

(29) Giester, G.; Lengauer, C. L.; Rieck, B. The crystal structure of nesquehonite, $\text{MgCO}_3 \cdot 3\text{H}_2\text{O}$, from Lavrion, Greece. *Mineral. Petrol.* **2000**, *70*, 153–163.

(30) Akao, M.; Iwai, S. The hydrogen bonding of hydromagnesite. *Acta Crystallogr.* **1977**, *33*, 1273–1275.

(31) Wang, Y. L.; Liu, J. Y.; Shi, T. J.; Li, C.; Wang, Q. H.; Zhang, J.; Zhu, Y. B.; Li, X. K.; Yuan, Z. G.; Yin, W. Z. Synthesis and pore structure construction mechanism of porous nesquehonite. *Powder Technol.* **2022**, *398*, 117154.

(32) Wang, Y. L.; Liu, J. Y.; Shi, T. J.; Wang, Q. H.; Zhang, J.; Zhu, Y. B.; Li, C.; Yuan, Z. G.; Yao, J.; Yin, W. Z. Synthesis, characterization and mechanism of porous spherical nesquehonite by CO_2 biomimetic mineralization. *Adv. Powder Technol.* **2022**, *33*, 103856.